Available online at www.sciencedirect.com
SCIENCE DIRECT
Journal of Catalysis 240 (2006) 100–107
JOURNAL OF CATALYSIS
www.elsevier.com/locate/jcat

Structure and oxidation state of gold on different supports under various CO oxidation conditions

N. Weiher [a,1], E. Bus [a], L. Delannoy [b], C. Louis [b], D.E. Ramaker [c], J.T. Miller [d], J.A. van Bokhoven [a,*]

[a] *Institute for Chemical and Bioengineering, Department of Chemistry and Applied Biosciences, ETH Zurich, Hönggerberg, 8093 Zurich, Switzerland*
[b] *Laboratoire de Réactivité de Surface, UMR 7609 CNRS, Université Pierre et Marie Curie, 4 place Jussieu, 75252, Paris cedex 05, France*
[c] *Chemistry Department, George Washington University, Washington, DC 20052, USA*
[d] *BP Research Center, 150 W. Warrenville Rd., Naperville, IL 60563, USA*

Received 25 November 2005; revised 10 February 2006; accepted 17 March 2006

Available online 24 April 2006

Abstract

The structure of gold clusters of different sizes supported on various metal oxides (Al_2O_3, TiO_2, SiO_2) exposed to different CO oxidation conditions was investigated in situ using X-ray absorption spectroscopy at the Au L_3 edge. In all catalysts, the only phase detected during catalysis was Au^0. In the most active sample with small gold particles (Au/Al_2O_3), variation in the electronic structure of the gold clusters with changing reaction conditions was observed by XANES spectroscopy and ascribed to the adsorption of CO on the metallic gold clusters. FEFF8 calculations proved that the changes in the XANES signature of Au/Al_2O_3 can be explained by backdonation of d-electrons into the π^* orbitals of CO. For Au/Al_2O_3, the presence of Au–O backscattering in the EXAFS suggested weak cluster–support interactions. For Au/SiO_2 and Au/TiO_2, the structure of the gold clusters remained unchanged throughout all experiments.

Keywords: X-ray absorption spectroscopy; Catalysis; Gold; Silica; Alumina; Titania; CO oxidation

1. Introduction

Supported gold nanoparticles catalyze various reactions, one of the most intensively studied of which is low-temperature CO oxidation, discovered by Haruta et al. [1]. Despite the great amount of research on this reaction, the structure of the active site remains ambiguous. The number of published reviews [2–8] demonstrates the complexity of this subject.

Although bulk gold does not react with H_2 or O_2, due to repulsion between the filled d-states of gold and the molecular orbitals of these molecules [9], small clusters can show extraordinary catalytic performance. The activity of supported gold catalysts strongly depends on the particle size [10–13]. Support materials can influence reactivity and are categorized as active (TiO_2, Fe_2O_3) or inactive (SiO_2, Al_2O_3) [14]. Active supports can provide oxygen atoms and thus enhance activity; however, they also enhance the stability of small gold particles [15]. The reactivity of Au clusters on inactive supports is attributed to the high dispersion of the metal and the presence of low-coordinated gold surface sites. Theoretical studies [16] confirm that low-coordinated gold atoms are essential for reactivity.

Many investigators have proposed Au^0 as the active species [17,18]. Au nanoparticles supported on a reducible oxide are considered essential for the genesis of active low-temperature oxidation catalysts. Bond and Thompson [2] proposed a mechanism involving unreduced gold species (Au^{III}) at the gold–support interface. Kung et al. found [19,20] that only very small gold particles supported on alumina are active in CO oxidation. They proposed that the reaction occurs on gold particles only but that it requires the presence of ensembles of Au^0 and Au^I–OH sites located at the metal–support interface [21]. In this mechanism, CO oxidation proceeds by reaction between O_2, which is dissociatively adsorbed on Au^0 and CO reacting

* Corresponding author. Fax: +41 44 632 1162.
E-mail address: j.a.vanbokhoven@chem.ethz.ch (J.A. van Bokhoven).
[1] Current address: School of Chemical Engineering and Analytical Science, The University of Manchester, Sackville Street, PO Box 88, Manchester, M60 1QD, United Kingdom.

0021-9517/$ – see front matter
doi:10.1016/j.jcat.2006.03.010

Table 1
Ex situ characterization and catalytic performance[a] of the materials used in this study

Sample	Support	Gold loading (wt%)	Cl content (wt%)	d_{avg}[c] (nm)	Conversion (% CO)	Rate ($mol_{CO}/(mol_{Au}\ s)$)	TOF[e] (s^{-1})
Au/Al_2O_3	Condea	0.30	< 0.2[b]	1.4	89	4.6×10^{-1}	1.8
Au/TiO_2	Degussa P25	0.63	< 0.2[b]	4.0[d]	83	1.6×10^{-1}	1.3
Au/SiO_2	Aerosil 300	1.00	< 0.2[b]	–	5	1.6×10^{-2}	0.1

[a] 300 K, 20 mL/min, 100 kPa total pressure, 3.3 kPa CO, 1.7 kPa O_2, balance He.
[b] Below detection limit of elemental analysis.
[c] Determined from TEM images.
[d] Bimodal particle size distribution, particle sizes 1–5 nm and 20–100 nm are detected.
[e] Estimated using the particle diameters derived from EXAFS.

with Au^I–OH, forming hydroxycarbonyls. The involvement of this Au^I–OH site is deduced from a careful study of the catalytic behavior of Au/γ-Al_2O_3 during deactivation and regeneration with water or hydrogen and the influence of water in the reactant feed [19]. Finally, based on free cluster studies, model catalyst investigations, and quantum chemical calculations [22–24], it has been found that charge transfer from F-centers to gold clusters occurs. Anionic gold species have been discussed as a possible cause of high activity [25–27].

The structure of active supported Au clusters—especially under in situ or operando conditions—has not been resolved unambiguously. Because most characterization techniques either probe the active site ex situ (TEM, XPS) or indirectly by measuring the interaction with probe molecules (CO chemisorption, IR), conclusions from such experiments may not be applicable to the working catalyst. Direct comparison of results from different research groups is often complicated by differences in the applied reaction conditions, such as the water content of the feed.

The present work characterizes the active site of multiple samples in situ under various reaction conditions and elucidates the structure and electronic state of the gold catalysts during reaction. XANES spectroscopy and FEFF8 calculations were applied to analyze and interpret changes in the electronic state of the Au clusters. The experiments demonstrate that, independent of support and reaction conditions, the dominant oxidation state of the Au clusters is zero. For the most active catalyst (Au/Al_2O_3), XANES difference spectra indicate backdonation of d-electron density from the Au clusters to π^* orbitals of adsorbed CO. EXAFS results show changes in the geometric structure of the Au clusters for Au/Al_2O_3.

2. Experimental

2.1. Sample preparation

Au/Al_2O_3 was prepared using a modified incipient wetness method. First, 100 mg of $HAuCl_4$ was dissolved in 5.1 mL of distilled water; then 10 g of sieved and dried Al_2O_3 (Condea, 0.125–0.250 μm) was added, and the system was shaken vigorously for 1 h. The resulting gray powder was poured into 200 mL of distilled water and heated to 340 K. The pH was maintained at 8 using 1 M NaOH. After stirring for 2 h, the solid was filtered, washed with hot water, and dried in vacuum at room temperature for 48 h.

Au/TiO_2 was prepared by deposition–precipitation. First, 400 mg of $HAuCl_4$ was dissolved in 200 mL of distilled water. The pH was adjusted to 7 using 1 M NaOH. Then 10 g of TiO_2 (P25, Degussa) was added, and the suspension was heated to 340 K. After 2 h of stirring, the solid was filtered and washed with hot water. The resulting powder was dried in vacuum at room temperature for 48 h.

Au/SiO_2 was prepared by incipient wetness impregnation of the support with an aqueous solution of $HAuCl_4$ (pH = 1). After impregnation, the sample was washed using aqueous ammonia (pH = 11) and deionized water and dried under vacuum at room temperature for 2 h.

The gold and chlorine content are reported in Table 1. The chlorine content is below the detection limit (<0.2 wt%) of elemental analysis in all samples.

2.2. Reduction procedure and reaction conditions

To activate the catalysts, all samples were reduced in a 5% H_2/He mixture before the CO oxidation experiments. This process was followed by in situ XANES spectroscopy. A heating rate of 5 K/min was used for all temperature ramps. Au/Al_2O_3 was reduced using a temperature step program with plateaus at 340, 370, 390, 420, 440, and 470 K. Each temperature was held for 30 min. Au/TiO_2 was reduced by heating to 370 K and holding the temperature for 1 h. Au/SiO_2 was reduced by using a temperature step program with plateaus at 320, 370, and 420 K; each temperature was held for 30 min. H_2 was removed by purging helium at the end temperature of the reduction for 30 min. The samples were allowed to cool to room temperature in a He flow of 20 mL/min. Subsequently, each sample was exposed to the same series of CO oxidation conditions (Table 2). All reactants were diluted to 5% in He. The $CO:O_2$ ratio was varied by changing the individual flow rates while keeping a total flow of 20 mL/min. On changing conditions, the samples were monitored using in situ XANES spectroscopy. After steady state was reached, full EXAFS spectra were recorded at the corresponding reaction temperature. No He purging was applied between different CO oxidation conditions. The water content of the stream was continuously monitored using a mass spectrometer and was comparable for all catalysts.

Table 2
Structural parameters elucidated from EXAFS

$CO:O_2$	1:1	2:1	1:2	1:1	1:2	2:1	He
$p(CO)$ (kPa)	2.5	3.3	1.7	2.5	3.3	1.7	0
$p(O_2)$ (kPa)	2.5	1.7	3.3	2.5	1.7	3.3	0
T (K)	300	300	300	370	370	370	300
			Au/Al_2O_3				
CN_{Au}	5.3	5.7	5.0	5.5	6.0	5.4	5.7
R_{Au} (Å)	2.73	2.73	2.77	2.76	2.76	2.75	2.77
σ^2_{Au} (10^{-3} Å^2)	14	14	10	15	15	13	13
$E_{0,Au}$ (eV)	2.4	2.2	1.1	0.5	1.3	0.9	1.0
CN_O	0.1	–	0.1	0.3	0.2	0.3	0.3
R_O (Å)	1.87	–	2.04	2.09	2.10	2.08	2.06
σ^2_O (10^{-3} Å^2)	8	–	7	8	11	9	14
$E_{0,O}$[a] (eV)	−5.5	–	−5.5	−5.5	−5.5	−5.5	−5.5
R-factor[b] (%)	6.8	–	3.6	4.4	3.1	2.4	5.8
			Au/TiO_2				
CN_{Au}	9.2	9.2	9.4	8.7	9.5	9.2	9.3
R_{Au} (Å)	2.84	2.84	2.84	2.84	2.84	2.84	2.84
σ^2_{Au} (10^{-3} Å^2)	8	7	8	8	9	9	8
$E_{0,Au}$ (eV)	4.7	3.9	4.3	3.8	4.2	3.9	3.3
R-factor[b] (%)	1.6	2.9	1.5	3.1	1.6	1.8	3.0
			Au/SiO_2				
CN_{Au}	7.1	6.3	6.5	6.7	6.2	7.0	7.2
R_{Au} (Å)	2.83	2.82	2.82	2.82	2.82	2.83	2.82
σ^2_{Au} (10^{-3} Å^2)	10	9	9	10	9	10	10
$E_{0,Au}$ (eV)	4.6	4.4	3.7	3.8	4.9	4.4	5.0
R-factor[b] (%)	2.5	3.6	1.8	2.9	3.5	4.1	2.8

Error margins are: CN ± 20%, σ^2 ± 20%, R ± 0.02 Å, E_0 ± 10%.
[a] E_0 of the Au–O shell constrained to the same value in all data sets.
[b] All data sets have been fitted using multiple k-weightings.

2.3. Transmission electron microscopy

TEM measurements were performed on a Tecnai F30 microscope (FEI Eindhoven). Fresh batches of Au/Al_2O_3 and Au/TiO_2 were reduced in H_2, dispersed in ethanol, and deposited onto a perforated carbon foil supported on a copper grid. Scanning transmission electron microscopy (STEM) images were obtained using a high-angle annular dark field (HAADF) detector that reveals the metal particles with bright contrast (Z-contrast).

2.4. X-ray absorption spectroscopy

All experiments were carried out at the BM01B station of the European Synchrotron Radiation Facility (ESRF), France. A plug-flow type in situ spectroscopic cell [28] was used for the experiments. Au L_3 XANES and EXAFS spectra were taken in fluorescence yield mode using a 13-element germanium detector. Higher harmonics were rejected using a Cr mirror. For each sample, the detector position was optimized to obtain the maximum S/N ratio. Care was taken to avoid saturation of the detector. One XANES scan was acquired every 15 min. Each EXAFS scan took 30 min; 4 spectra were averaged to improve the S/N ratio. All data were analyzed using the IFEFFIT library [29] and its front ends ATHENA and ARTEMIS [30]. The overall amplitude reduction factor, S_0^2, was determined by fitting a gold foil EXAFS using a fixed coordination number (CN) of 12; it was kept fixed at a value of 0.83 while all other spectra were fitted. Reference paths were calculated using the crystal structures of Au (Au–Au shell) [31] and Au_2O_3 (Au–O shell) [32] using the FEFF8 code [33]. EXAFS fits have been performed simultaneously in k-weightings of one, two and three to avoid introducing errors with regard to the coordination numbers and Debye–Waller factors.

Full multiple scattering calculations were performed with the FEFF8 code [33]. The gold cluster used in the calculations consisted of six gold atoms positioned in two layers—four in the first and two on top. This cluster contains atop, bridged, HCP, and FCC adsorption sites [34]. The CO molecule was placed on an atop site, and a geometry optimization using force field calculations with the HYPERCHEM software [35] was performed. After optimization, the Au–CO distance was 2.0 Å. Full multiple scattering FEFF simulations were carried out using self-consistent field Hedin–Lundqvist potentials. This procedure was carried out for all possible adsorption sites.

3. Results

3.1. Catalytic performance and ex situ characterization

Table 1 summarizes the properties and catalytic performance of the investigated samples. The gold loading was determined using atomic absorption spectroscopy. Conversions and reaction rates were extracted from mass spectrometer traces, measured during the XAS experiments. The turnover frequencies were estimated assuming hemispherical particles with sizes derived from EXAFS analysis (vide infra). A stoichiometric mixture of 3.3 kPa CO and 1.7 kPa O_2 (balance He) at a total flow rate of 20 mL/min and 300 K was used to determine these values. Au/Al_2O_3 and Au/TiO_2 showed the highest CO conversion; Au/SiO_2 was less reactive. Under the applied conditions, Au/Al_2O_3 and Au/TiO_2 showed almost 100% conversion. Therefore, the rates and turnover frequencies for these samples are underestimated.

Fig. 1 shows a TEM image of Au/Al_2O_3 taken after reduction of the catalyst. Most of the Au particles had a diameter of 1–2 nm; the average particle size was 1.4 nm. For Au/TiO_2, TEM showed a bimodal particle size distribution. Most particles were 1–5 nm in diameter; few particles were 20–100 nm in diameter.

3.2. Catalyst reduction

Fig. 2 shows in situ Au L_3 XANES data obtained during catalyst reduction. The marks correspond to the edge position of Au foil (A), the whiteline position of Au^{3+} (B), and isobestic points observed during the reduction (C–E). The first (before reduction) and last (fully reduced sample) spectra are marked bold; dashed spectra were acquired every 15 min. Reference spectra of Au_2O_3 and Au^0 are given. For all catalysts except Au/TiO_2, the spectra obtained before reduction showed the typical high white line of trivalent cationic gold species such as Au_2O_3 and $AuCl_3$ [36,37], which decreased monotonically during the reduction process.

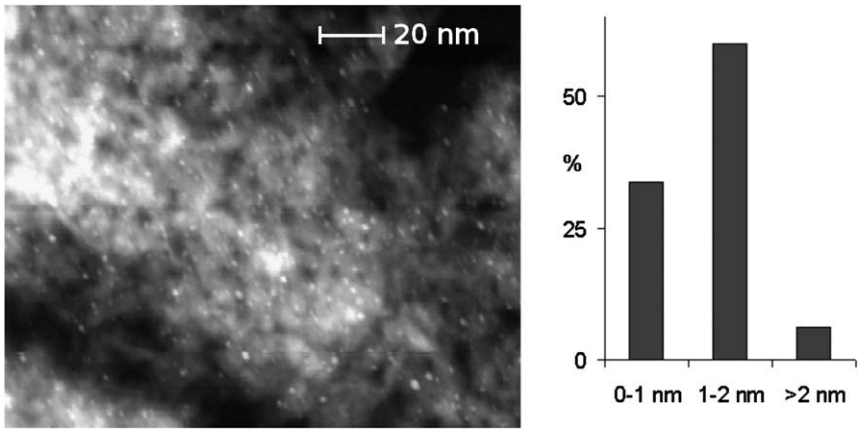

Fig. 1. TEM picture and particle size distribution of Au/Al_2O_3.

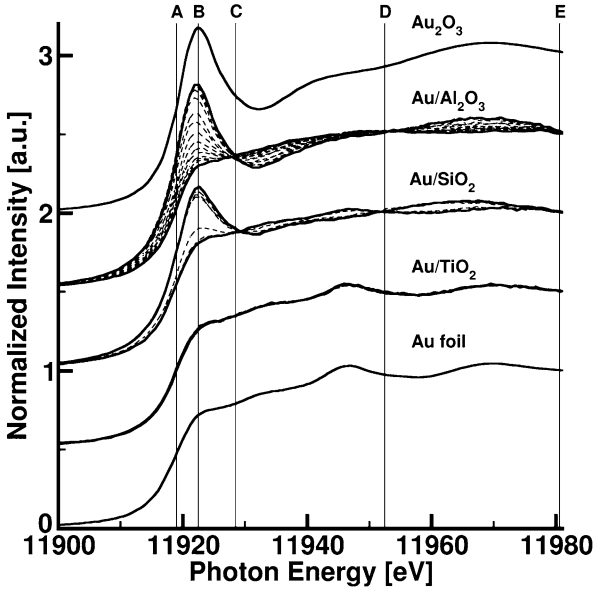

Fig. 2. In situ XANES spectra acquired during sample reduction. Reference spectra for Au_2O_3 and Au^0 are given. Bold lines depict the first and last spectrum of the series, dashed spectra are taken in intervals of 15 min.

Au/Al_2O_3 was fully reduced at 470 K. Characteristic spectral features of the reduced sample are (i) an edge position of 11,919 eV, (ii) a shoulder at 11,930 eV, and (iii) peaks at 11,947 and 11,970 eV. These features are located at identical energy positions as in the spectrum of metallic gold but show a lower intensity [38]. For Au/SiO_2, reduction started at 320 K and was complete at 420 K. Au/TiO_2 showed the characteristic features of Au^0 before the H_2 treatment, and no further changes were observed.

3.3. In situ characterization of the active site

Fig. 3a shows the Au L_3 XANES spectra of all reduced catalysts exposed to atmospheres with varying $CO:O_2$ ratios (cf. Table 2). The gas mixture was added to the previously reduced catalysts. For Au/TiO_2 and Au/SiO_2, the shape of the XANES was independent of gas composition and temperature. For Au/Al_2O_3, the XANES spectra varied with reaction condi-

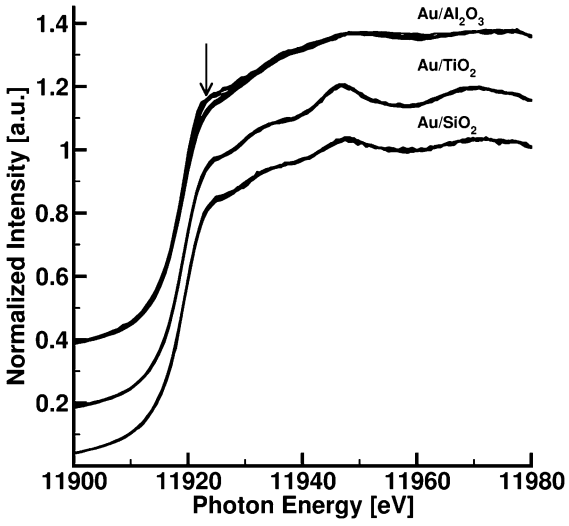

(a)

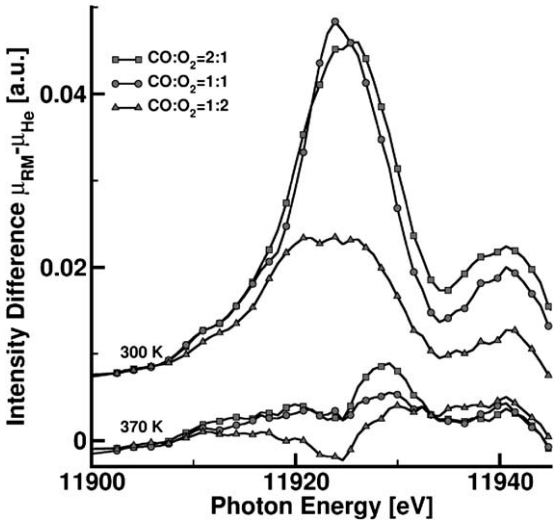

(b)

Fig. 3. (a) XANES region of the reduced catalysts during different CO oxidation conditions. The arrow denotes the position where changes are visible for Au/Al_2O_3. For partial pressures of the reactants refer to Table 2. (b) XANES difference spectra (calculated as spectrum under reaction conditions − reference in He at 300 K) for the reduced Au/Al_2O_3 catalyst exposed to different CO oxidation conditions. For partial pressures of the reactants refer to Table 2.

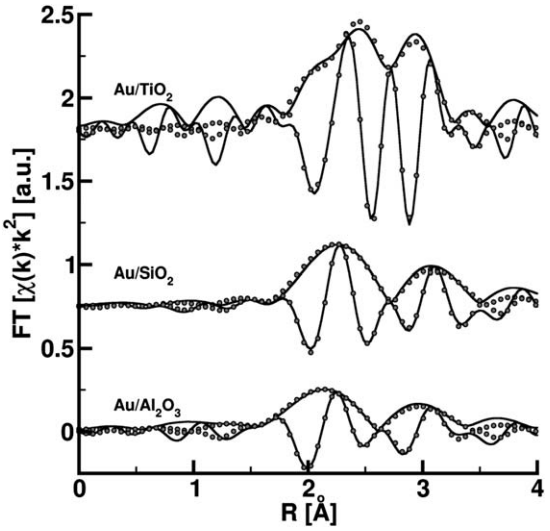

Fig. 4. Magnitude and imaginary part of the k^2-weighted Fourier transformed EXAFS data (lines) and fits (dots) for all reduced catalysts in He at 300 K.

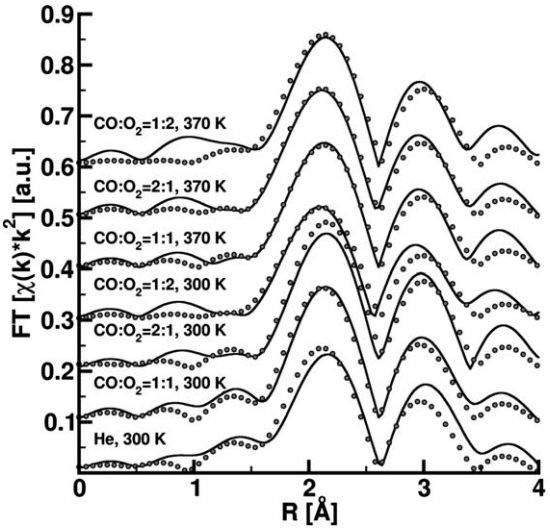

Fig. 5. Magnitude of the k^2-weighted Fourier transformed EXAFS data (lines) and fits (dots) for Au/Al_2O_3 under different reaction conditions.

tions. Difference spectra between the data taken under reaction conditions and a reference spectrum recorded in He at 300 K are shown in Fig. 3b. The XANES intensity at 11,923 eV clearly increased with increasing CO concentration in the gas feed at 300 K and less pronouncedly so at 370 K.

Fig. 4 shows the Fourier-transformed k^2-weighted Au L_3 EXAFS spectra of the reduced catalysts in He at 300 K. Fit results are given in Table 2. Fits were performed in R-space using Hanning windows for the Fourier filtering. The following parameters were applied: $k = [3{:}8.5]$ Å^{-1}, $R = [1{:}4]$ Å, $\Delta k = 0.4$ Å^{-1}, and $\Delta R = 0.4$ Å. Fits were performed using multiple k-weightings of one, two and three to avoid artifacts introduced by the fitting and background subtraction process. This was important to obtain reliable coordination numbers and Debye–Waller factors, because different combinations of these parameters can yield similar fit qualities in different k-weightings. In all cases the R-factors did not change significantly with k-weighting; the R-factors given in Table 2 present average values of the three individual fits. We can safely state that the values given in Table 2 represent our data well in all different k-weightings. For all samples, we observed the typical features for Au–Au backscattering between 2 and 4 Å. Au/TiO_2 and Au/SiO_2 showed only Au–Au backscattering contributions. In the case of Au/Al_2O_3, adding Au–O backscattering contributions improved the quality of the fit. According to Nyquist's theorem, the k- and R-range applied in the fitting process corresponds to 9 degrees of freedom. Fitting two independent shells required eight variables (E_0, R, σ^2 and R for each shell), and because the Au–O contribution was small, the variables obtained for it were on the border of statistical significance. Au/TiO_2 exhibited a high Au–Au CN (about 9), whereas the other catalysts showed significantly lower values (about 6). In all cases, a stable fit was obtained by varying all shell parameters at the same time.

Au/SiO_2 showed no variation of structure with reaction conditions. The average CN of 6.5 indicated a particle size of slightly below 1 nm. A contraction of the Au–Au bond distance compared with bulk gold was observed. Au/TiO_2 showed a less pronounced Au–Au distance contraction and higher CN. The size of the gold clusters was estimated as 2 nm. Fig. 5 shows the Fourier-transformed k^2-weighted EXAFS data and fits of Au/Al_2O_3 under various reaction conditions. This sample differs from Au/TiO_2 and Au/SiO_2 in terms of more pronounced changes in the Au–Au distance and the presence of Au–O backscattering contributions of varying intensity. It also has the smallest Au particle sizes, with CNs between five and six. At 300 K, the contribution of Au–O was more pronounced in He (0.3) than in the reaction mixture (0.1).

3.4. Simulation of reactant adsorption on gold clusters

Full multiple scattering calculations with the FEFF8 code are frequently used to interpret experimental XANES data [39]. Fig. 6a shows the calculated Au L_3 XANES spectra of a Au_6 cluster [34] with and without adsorbed CO. The XANES was calculated for the atom that bonds directly to the CO molecule (Fig. 6b). Other adsorption sites were investigated but are not reported here, because the differences between the corresponding spectra were small. All possible adsorption sites exhibited a white line comparable to that shown in Fig. 6a. The spectrum of the bare Au_6 cluster resembled that of bulk gold except for the lower intensity of the features. For the cluster-adsorbate complex, the FEFF simulation showed a significant white line intensity.

4. Discussion

4.1. Catalytic activities and ex situ characterization

Of the three catalysts studied, Au/Al_2O_3 performed the best, followed by Au/TiO_2 and Au/SiO_2 (Table 1). Note that Au/SiO_2 demonstrated catalytic activity, although at an order of magnitude less than that of Au/Al_2O_3 and Au/TiO_2. Our data compare well with that of Costello et al. [19] and Kung et

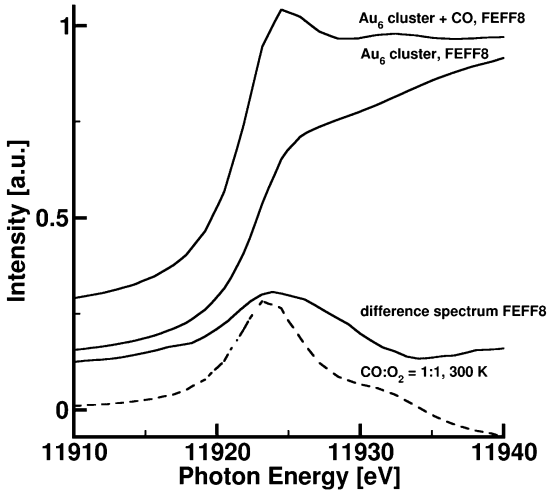

(a)

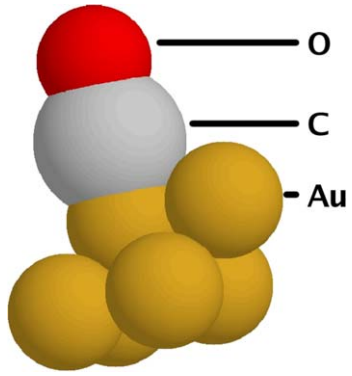

(b)

Fig. 6. (a) FEFF8 simulations of a Au_6 cluster and a Au_6 cluster with CO adsorbed on an atop site. One experimental difference spectrum ($CO:O_2 = 1:1$, 300 K) is given as a dashed line. (b) Optimized geometry of the Au_6–CO cluster used for the FEFF8 calculations shown in (a).

al. [20]. Our finding that Au/Al_2O_3 is more active than Au/TiO_2 can be explained by the difference in particle size between these samples. Au/Al_2O_3 contains smaller, and thus more reactive, gold clusters compared with Au/TiO_2. Although the average Au clusters on TiO_2 are significantly larger than those on Al_2O_3, Au/TiO_2 shows high activity. This can be explained by the bimodal particle size distribution found via TEM. Small particles (1–5 nm) cause the activity of this sample, whereas the large particles (20–100 nm) act as spectator species. The performance of our catalysts compares with those reported in the literature.

4.2. Structure of the active site after reduction

Unreduced Au/SiO_2 and Au/Al_2O_3 exhibited slightly different white line intensities before reduction; Au/TiO_2 was already reduced before H_2 treatment (Fig. 2). Nonreduced Au on Al_2O_3 [40] and TiO_2 [41] is known to be inactive in CO oxidation; therefore, a reductive treatment is needed to obtain high catalytic activities, and also to ensure comparable cluster properties before catalytic measurements. Au/TiO_2 showed pronounced XANES features similar to those found for bulk gold. In all other samples, the XANES was less structured. Because the intensity of spectral features is proportional to the number of backscattering atoms present [42], the Au clusters in Au/TiO_2 are significantly larger than those in Au/Al_2O_3 or Au/SiO_2.

Schwartz et al. [13] reported the presence of large, fully reduced gold particles in Au/TiO_2-based CO oxidation catalysts. They detected only zero-valent gold during CO oxidation; however, the Au particles in their catalyst were rather large, and thus detecting changes in the small amount of active gold might not have been possible. In their study, the as-prepared catalyst contained Au^{3+}. Yang et al. [41] studied the activation of Au/TiO_2 using H_2 and CO pulse reduction and concluded that metallic gold is necessary to obtain active catalysts. Their XAS results demonstrated the initial presence of Au^{3+} species, which are reduced to metallic gold during the activation process.

Our observation of reduced Au particles before H_2 treatment can be explained by the high sensitivity of Au/TiO_2 to light. Exposure to light during the transfer of the sample into the reactor or to the X-ray beam may have induced autoreduction. The reduction behavior of Au/Al_2O_3 is in line with the results of Calla and Davis [43–45]. The findings of our EXAFS analysis are in agreement with their results regarding the particle sizes. Costello et al. studied the activation of Au/Al_2O_3 using XAS and TPR studies [40]. Our catalyst showed a similar reduction behavior; elevated temperatures are necessary to completely reduce the gold particles. The presence of isobestic points in the reduction of Au/Al_2O_3 and Au/SiO_2 suggests that gold is present as either Au^{3+} or Au^0 during the reduction. Jansen [32] stated that Au_2O_3 is the only unambiguously characterized binary gold oxide. Oxides of other oxidation states are less stable and not likely to form under the conditions applied in our experiments. Therefore, the reduction behavior of the materials is consistent with the chemistry of bulk gold oxides.

The EXAFS spectra of Au/TiO_2 and Au/SiO_2 (Fig. 4) were dominated by Au–Au backscattering (Table 2). In agreement with the intensity of the XANES features, Au/TiO_2 had the highest Au–Au CN. Although Au/SiO_2 exhibited small particle sizes, no gold–support oxygen or gold–adsorbate backscattering could be observed. For Au/Al_2O_3 (Fig. 5), a minor Au–O backscattering contribution with CNs < 0.3 can be ascribed to oxygen atoms of the support. For this catalyst, the particle size determined via EXAFS (Table 2) was in good agreement with the TEM results (Table 1, Fig. 1). Goodman [46] discussed Au/TiO_2 as an example for strong metal–support interactions, which should lead to well-defined Au–O or Au–Ti shells. Because XAS is a bulk technique, these contributions are visible only if the clusters are sufficiently small, which is not the case with our Au/TiO_2 catalyst. In all samples, the Au–Au distance was smaller than in bulk gold (2.88 Å), an effect that has been documented for other metal clusters [47,48].

4.3. Structure of the active site determined under reaction conditions

For Au/TiO_2 and Au/SiO_2, neither the XANES nor the EXAFS data showed clear trends when the CO oxidation conditions were varied (Fig. 3a, Table 2). However, none of the

catalysts was truly inactive, so at least weak interactions between gold and reactants were expected. In these cases, the concentration of sites exhibiting structural variations might be too low to allow detection by XAS. Au/Al_2O_3 showed pronounced changes in the XANES signature between 11,920 and 11,940 eV on variation of the CO oxidation conditions (Fig. 3b). The intensity was highest at the highest CO concentration and lower at higher temperatures. One possible cause of these changes is Au cluster reoxidation. Literature data demonstrate that Au^{3+} compounds such as $AuCl_3$ or Au_2O_3 show a white line at 11,923 eV [36,37] (Fig. 2). Should reoxidation cause the observed changes, then a correlation between white line intensity and O_2 concentration would be expected; however, the highest white line intensities were observed in the presence of excess CO. Recent work [49] showed that spectra of supported gold catalysts exhibit a small white line after chemisorption of H_2. Our FEFF8 calculations showed that the shape of the difference spectra obtained during CO oxidation can be explained by backdonation of d-electron density from the Au cluster to CO (Figs. 6a and b). Studies on the interaction of Au(110) with CO by Gottfried et al. confirmed that CO interacts with gold single crystals [50]. Winkler et al. studied the interaction of carbon monoxide with gold clusters adsorbed on γ-Al_2O_3 single crystals [51] and concluded that CO adsorbs on zero-valent gold clusters. We found a lower white line intensity at 370 K than at 300 K, suggesting lower CO coverage at higher temperatures. This can be explained by a shift of the thermal equilibrium (i.e., less CO adsorbs at higher temperatures).

With respect to the oxidation state of gold in low-temperature oxidation catalysts, a broad range of experimental data and opinions exists [17,18,22–26,52–56]. Haruta and coworkers [17,18] concluded that small zero-valent clusters cause the high activity of supported gold catalysts. Evidence for negatively polarized gold in CO oxidation catalysts has been reported [22–26]. Several authors have reported the presence of cationic gold clusters [52–56]. Some have claimed that cationic gold is present along with zero-valent gold [52,53,55]; others have claimed that *only* cationic gold can be active [54]. Following this hypothesis, in an article describing a highly active Au/La_2O_3 CO oxidation catalyst, Fierro-Gonzalez et al. [56] questioned whether zero-valent gold is in fact necessary for generating high activity. These authors claimed that the XANES spectrum of the catalyst showed only characteristics of Au^{3+}. The XANES spectra of Au^{3+} species exhibit very high white line intensities, as shown by the spectrum of Au_2O_3 in Fig. 2. In contrast, the XANES spectrum reported by Fierro-Gonzalez et al. [56] showed a strongly reduced white line intensity and resembled the intermediate spectra obtained during catalyst reduction shown in our Fig. 2. This is unmistakable evidence for the presence of lower oxidation states. In all catalysts investigated in the present study—especially the most active one, Au/Al_2O_3—only zero-valent gold was detected in situ under various CO oxidation conditions. Our results suggest that in the materials investigated, fully reduced gold was the active species in the oxidation of CO. This conclusion agrees with those of previous reports [13,17,18,43–45]. No evidence for cationic gold species in active CO oxidation catalysts was found, although we cannot rule out that such species may be formed under certain conditions.

Au/Al_2O_3 and Au/SiO_2 exhibited similar gold cluster sizes. Although trends in the electronic structure of Au/Al_2O_3 with varying reaction conditions were observed via XANES spectroscopy (Fig. 3b), such trends were absent in Au/SiO_2. This finding is consistent with the observation that this catalyst was less active; reactant adsorption on the gold clusters was not favored in this material. The support influenced the activity of the gold clusters in Au/Al_2O_3, and weak Au–O interactions were detected (the presence of an Au–O contribution in Table 2). Previous studies have shown that the support can affect the preferred adsorption sites on small metal particles [57]. Argo et al. [58] suggested that the support behaves as a ligand that affects the metal particles. Valden et al. [59] correlated the onset of catalytic activity with the appearance of nonmetallic properties in Au/TiO_2. Ramaker et al. [60] reported that the metal to insulator transition in supported metal particles is a function of the support. We did not detect any changes in the active site of Au/TiO_2, which can be explained by the larger average particle size and bimodal particle size distribution observed via TEM. In Au/Al_2O_3, the small average particle size and narrow particle size distribution facilitated observation of changes in electronic and geometric structure.

5. Conclusion

Here we report a detailed study of the structure of the active site of various supported gold catalysts. The presence of isobestic points observed in the XAS during catalyst reduction suggests that the reduction proceeds directly from Au^{3+} to Au^0 without passing other oxidation states. For Au/Al_2O_3, we detected CO adsorption manifesting as changes in the electronic structure of the gold cluster on variation of reactant stoichiometry. A correlation between CO concentration and whiteline intensity can be attributed to backdonation of d-electron density from the metallic gold cluster to CO. Small cluster–support interactions were detected for this sample. Such trends were not observed for Au/SiO_2, which is consistent with this catalyst's lower reactivity. For Au/TiO_2, the large gold particles prevented detection of structural changes by XAS. It is important to stress that in all of the materials studied, only metallic gold was detected during the catalytic oxidation of CO.

Acknowledgments

The authors thank the ESRF for providing beam time at station BM01B, as well as the station scientists (H. Emerich and W. van Beek) for their support. This project was supported by the Swiss National Science Foundation (NW, JAvB) and the European Union under contract HPRN-1999-00151.

References

[1] M. Haruta, T. Kobayashi, H. Sano, N. Yamada, Chem. Lett. 2 (1987) 405.
[2] C.G. Bond, D.T. Thompson, Gold Bulletin 33 (2000) 41.

[3] M. Haruta, M. Daté, Appl. Catal. A 222 (2001) 427.
[4] M. Haruta, Cattech 6 (2002) 102.
[5] M. Haruta, Chem. Record 3 (2003) 75.
[6] M. Haruta, J. New Mater. Electrochem. Systems 7 (2004) 163.
[7] G.J. Hutchings, Catal. Today 100 (2005) 55.
[8] R. Meyer, C. Lemire, S.K. Shaikhutdinov, H.-J. Freund, Gold Bulletin 37 (2004) 72.
[9] B. Hammer, J.K. Nørskov, Nature 376 (1995) 238.
[10] A.I. Kozlov, A.P. Kozlova, K. Asakura, Y. Matsui, T. Kogure, T. Shido, Y. Iwasawa, J. Catal. 196 (2000) 56.
[11] M. Haruta, S. Tsubota, T. Kobayashi, H. Kageyama, M.J. Genet, B. Delmon, J. Catal. 144 (1993) 175.
[12] R. Zanella, S. Giorgio, C.-H. Shin, C.R. Henry, C. Louis, J. Catal. 222 (2004) 357.
[13] V. Schwartz, D.R. Mullins, W.F. Yan, B. Chen, S. Dai, S.H. Overbury, J. Phys. Chem. B 108 (2004) 15782.
[14] M.M. Schubert, S. Hackenberg, A.C. van Veen, M. Muhler, V. Plzak, R.J. Behm, J. Catal. 197 (2001) 113.
[15] A. Gluhoi, N. Bogdanchikova, B.E. Nieuwenhuys, Gold 2003, Vancouver.
[16] I.N. Remediakis, N. Lopez, J.K. Nørskov, Angew. Chem. Int. Ed. 44 (2005) 1824.
[17] M. Okumura, S. Nakamura, S. Tsubota, T. Nakamura, M. Azuma, M. Haruta, Catal. Lett. 51 (1998) 53.
[18] M. Okumura, S. Tsubota, M. Haruta, J. Mol. Catal. A: Chem. 199 (2003) 73.
[19] C.K. Costello, M.C. Kung, H.-S. Oh, H.H. Kung, Appl. Catal. A 232 (2002) 159.
[20] H.H. Kung, M.C. Kung, C.K. Costello, J. Catal. 216 (2003) 425.
[21] C.K. Costello, J.H. Yang, H.Y. Law, Y. Wang, J.N. Lin, L.D. Marks, M.C. Kung, H.H. Kung, Appl. Catal. A 243 (2003) 15.
[22] L.D. Socaciu, J. Hagen, T.M. Bernhardt, L. Woste, U. Heiz, H. Häkkinen, U. Landman, J. Am. Chem. Soc. 125 (2003) 10437.
[23] A. Sanchez, S. Abbet, U. Heiz, W.-D. Schneider, H. Häkkinen, R.N. Barnet, U. Landman, J. Phys. Chem. A 103 (1999) 9573.
[24] H. Häkkinen, S. Abbet, A. Sanchez, U. Heiz, U. Landman, Angew. Chem. Int. Ed. 42 (2003) 1297.
[25] Z. Yan, S. Chinta, A.A. Mohamed, J.P. Fackler, D.W. Goodman, J. Am. Chem. Soc. 127 (2005) 1604.
[26] B. Yoon, H. Häkkinen, U. Landman, A.S. Wörz, J.-M. Antonietti, S. Abbet, K. Judai, U. Heiz, Science 307 (2005) 403.
[27] L.D. Socaciu, J. Hagen, T.M. Bernhardt, L. Woste, U. Heiz, H. Häkkinen, U. Landman, J. Am. Chem. Soc. 125 (2003) 10437.
[28] N. Weiher, E. Bus, B. Gorzolnik, M. Möller, R. Prins, J.A. van Bokhoven, J. Syn. Rad. 12 (2005) 675.
[29] M. Newville, J. Syn. Rad. 8 (2001) 96.
[30] B. Ravel, M. Newville, J. Syn. Rad. 12 (2005) 537.
[31] E.R. Jette, F. Foote, J. Chem. Phys. 3 (1935) 605.
[32] M. Jansen, A.V. Mudring, Gold: Progress in Chemistry, Biochemistry and Technology, Wiley, 1999.
[33] A.L. Ankudinov, B. Ravel, J.J. Rehr, S.D. Conradson, Phys. Rev. B 58 (1998) 7565.
[34] E. Janin, H. von Schenck, M. Göthelid, U.O. Karlsson, M. Svensson, Phys. Rev. B 61 (2000) 13144.
[35] W.F. Coleman, C.R. Arumainayagam, J. Chem. Educ. 75 (1998) 416.
[36] N. Weiher, E.A. Willneff, C. Figulla-Kroschel, M. Jansen, S.L.M. Schroeder, Sol. State Commun. 125 (2003) 317.
[37] A. Pantelouris, G. Küper, J. Hormes, C. Feldmann, M. Jansen, J. Am. Chem. Soc. 117 (1995) 11749.
[38] T.M. Salama, T. Shido, R. Ohnishi, M. Ichikawa, J. Phys. Chem. 100 (1996) 3688.
[39] A. Teliska, W.E. O'Grady, D.E. Ramaker, J. Phys. Chem. B 109 (2005) 8076.
[40] C.K. Costello, J. Guzman, J.H. Yang, Y.M. Wang, M.C. Kung, B.C. Gates, H.H. Kung, J. Phys. Chem. B 108 (2004) 12529.
[41] J.H. Yang, J.D. Henao, M.C. Raphulu, Y. Wang, T. Caputo, A.J. Groszek, M.C. Kung, M.S. Scurrell, J.T. Miller, H.H. Kung, J. Phys. Chem. B 109 (2005) 10319.
[42] D.C. Koningsberger, B.L. Mojet, G.E. van Dorssen, D.E. Ramaker, Top. Catal. 10 (2000) 143.
[43] J.T. Calla, R.J. Davis, J. Phys. Chem. B 109 (2005) 2307.
[44] J.T. Calla, R.J. Davis, Catal. Lett. 99 (2005) 21.
[45] J.T. Calla, R.J. Davis, Ind. Eng. Chem. Res. 44 (2005) 5403.
[46] D.W. Goodman, Catal. Lett. 99 (2005) 1.
[47] G. Apai, J.F. Hamilton, J. Stohr, A. Thompson, Phys. Rev. Lett. 43 (1979) 165.
[48] B. Delley, D.E. Ellis, A.J. Freeman, E.J. Baerends, D. Post, Phys. Rev. B 27 (1983) 2132.
[49] E. Bus, J.T. Miller, J.A. van Bokhoven, J. Phys. Chem. B 109 (2005) 14581.
[50] J.M. Gottfried, K.J. Schmidt, S.L.M. Schroeder, K. Christmann, Surf. Sci. 536 (2003) 206.
[51] C. Winkler, A.J. Carew, S. Haq, R. Raval, Langmuir 19 (2003) 717.
[52] J. Guzman, B.C. Gates, J. Am. Chem. Soc. 126 (2004) 2672.
[53] J. Guzman, B.C. Gates, J. Phys. Chem. B 106 (2002) 7659.
[54] J.C. Fierro-Gonzales, B.C. Gates, J. Phys. Chem. B 108 (2004) 16999.
[55] J. Guzman, B.C. Gates, J. Phys. Chem. B 107 (2003) 2242.
[56] J.C. Fierro-Gonzalez, V.A. Bhirud, B.C. Gates, Chem. Commun. 42 (2005) 5275.
[57] D.C. Koningsberger, M.K. Oudenhuijzen, J. de Graaf, J.A. van Bokhoven, D.E. Ramaker, J. Catal. 216 (2003) 178.
[58] A.M. Argo, J.F. Odzak, F.S. Lai, B.C. Gates, Nature 415 (2002) 623.
[59] M. Valden, X. Lai, D.W. Goodman, Science 281 (1998) 1647.
[60] D.E. Ramaker, M.K. Oudenhuijzen, D.C. Koningsberger, J. Phys. Chem. B 109 (2005) 5608.